Atmos. Chem. Phys. Discuss., 12, 15177–15225, 2012
www.atmos-chem-phys-discuss.net/12/15177/2012/
doi:10.5194/acpd-12-15177-2012

Atmospheric Chemistry and Physics Discussions

Soot and SO_2 contribution to the supersites in the MILAGRO campaign from elevated flares in the Tula Refinery

V. H. Almanza[1], L. T. Molina[2,3], and G. Sosa[1]

[1]Instituto Mexicano del Petróleo, 07730 México, DF, Mexico
[2]Molina Center for Energy and the Environment, La Jolla, CA, USA
[3]Department of Earth, Atmospheric and Planetary Sciences, Massachusetts Institute of Technology, Cambridge, MA, USA

Received: 5 April 2012 – Accepted: 22 May 2012 – Published: 14 June 2012

Correspondence to: G. Sosa (gsosa@imp.mx)

Published by Copernicus Publications on behalf of the European Geosciences Union.

Abstract

This work presents a simulation of the plume emitted by flaring activities of the Miguel Hidalgo Refinery in Mexico. The flame of a representative sour gas flare is modeled with a CFD combustion code in order to estimate emission rates of combustion by-products of interest for air-quality: acetylene, ethylene, nitrogen oxides, carbon monoxide, soot and sulfur dioxide. The emission rates of NO_2 and SO_2 were compared against measurements obtained at Tula as part of MILAGRO field campaign. The rates of soot, VOCs and CO were compared with estimates obtained by IMP. The emission rates of the species considered were further included in WRF-Chem model to simulate the chemical transport of the plume from 22 March to 27 March of 2006. The model presents reliable performance of the resolved meteorology, with respect to the Mean Absolute Error (MAE), Root Mean Square Error (RMSE), vector RMSE and Index of Agreement (IOA).

WRF-Chem outputs of $SO_2$and soot were compared with surface measurements obtained at the three supersites of MILAGRO campaign. The results suggest a contribution of Tula flaring activities to the total SO_2 levels of 23 % to 37 % at the urban supersite (T0), and of 29 % to 39 % at the suburban supersite (T1). For soot, the model predicts low contribution at the three supersites, with less than 1 % at both T0 and T1; and about 1 % at T2. According to the model, the greatest contribution of both pollutants to the three supersites occurred on 23 March, which coincides with the third cold surge event.

1 Introduction

Flaring is an important source of greenhouse gases, particulate matter and Volatile Organic Compounds (VOCs) in both upstream and downstream operations in the oil and gas industry. About 134 billion cubic meters (bcm) of gas were flared in 2010 according to the World Bank Global Gas Flaring Reduction Initiative (GGFR) estimates of flared

ACPD
12, 15177–15225, 2012

volume from satellite data (GGFR, 2012). This represents up to 400 million metric tons of CO_2 eq global greenhouse gas emissions. In 2010 Mexico was the eleventh emitting country with 2.5 bcm (World Bank, 2012). The US Energy Information Administration (EIA) estimates about 17 million metric tons of CO_2 eq emitted from flaring of natural gas for Mexico in 2009 (US EIA, 2012).

The composition of the gas to be flared depends on process operations. It may contain heavier hydrocarbons, water vapor, hydrogen sulfide, nitrogen, and carbon dioxide principally (GE Energy, 2011). As a result, harmful by-products such as NO_x, reactive organic gases (ROG), polycyclic aromatic hydrocarbons (PAHs), sulfur dioxide and soot are emitted to the atmosphere.

Black carbon (a component of soot) emissions from flaring facilities are of particular interest because of their harmful effect to air quality and contribution to both global and regional climate change (Chung and Seinfeld, 2005). It can warm the atmosphere, reduces surface albedo on ice surfaces accelerating snow melt, affects clouds, slows convection and impacts the hydrological cycle (Skeie et al., 2011; McMeeking et al., 2011; Kahnert et al., 2011). In terms of global warming potential, black carbon is second to CO_2 (Moffet and Prather, 2009); since its atmospheric lifetime is short (days to weeks) with respect to CO_2, it is considered a short-lived climate forcer (SLCF) (UNEP, 2011). This feature promotes a rapid climate response when changing emissions. Thus, control of black carbon particles by emission reduction measures would have immediate benefits on air quality and global warming (Bond et al., 2011; UNEP, 2011). Therefore, having robust estimates of emission rates of soot can be helpful in improving emission inventories for air quality modeling.

In Mexico, flaring operations are basically associated with activities of exploration, exploitation, refining and petrochemical operations of PEMEX, the national oil company. These are geographically located in the eastern coast along the Gulf of Mexico (Tamaulipas, Veracruz and Tabasco); in the southeastern part of the country (the Campeche sound), and in the central region of the country (Guanajuato, Hidalgo and Oaxaca states). In this work we focus on flaring emissions from the Tula refinery

ACPD
12, 15177–15225, 2012

(Hidalgo State) during MILAGRO campaign (Molina et al., 2010). The motivation to focus on flaring operations is twofold: (i) to infer about the contribution of the emissions by elevated flares on pollution levels; (ii) to assess the viability to further extend the present investigation to different flaring activities of PEMEX.

1.1 Tula region

The city of Tula is located in the Mezquital Valley, in southwest Hidalgo with a total population of nearly 94 000 inhabitants and more than 140 industries. The region is semi-arid with average temperatures of 17 °C and precipitation ranging from 432 to 647 mm, increasing from north to south. In this region, the Tula Industrial Complex (TIC) is settled in an area of 400 km^2. The major industries of the city are located within this region, including the Miguel Hidalgo Refinery (MHR), the Francisco Perez Rios power plant (FPRPP), several cement plants and limestone quarries. Other minor industries include metal manufacturing, processed food, chemical and incineration of industrial waste. The emission of pollutants from combustion processes of these industries impacts the regional air quality. In addition, the inflow of untreated sewage water from Mexico City promotes severe pollution problems to soil and water resources (Cifuentes et al., 1994; Vazquez-Alarcón et al., 2001). According to current environmental regulations, this region is classified as a critical area due to the high emissions of SO_2 and particulate matter (SEMARNAT-INE, 2006).

The Mexican Ministry of the Environment and Natural Resources (SEMARNAT) brought the attention to the Tula area for two main reasons: (1) its relative closeness to Mexico City (60 km NW); (2) environmental authorities of the State of Mexico sued the two major industries in the region at the beginning of 2006. They claimed that the high levels of pollutants registered in the Automatic Atmospheric Monitoring Network (RAMA) stations were consequence of their emissions. In this respect, the RAMA has been reported high concentrations of SO_2 in the northern area of Mexico City that can exceed the national air quality standard (0.13 ppm, 24-h average). According to the latest emission inventory in this region, the emissions rates are about 323 000 tons yr^{-1}

ACPD
12, 15177–15225, 2012

of SO_2; 109 321 tons yr^{-1} of CO; 44 265 tons yr^{-1} of NO_x; 22 671 tons yr^{-1} of PM and 44 632 tons yr^{-1} of VOCs.

This has motivated several research studies evaluating the influence of Tula emissions on regional air quality, particularly in Mexico City (Querol et al., 2008; Rivera et al., 2009; de Foy et al., 2006). For instance, de Foy et al. (2009a) analyzed the influence of the SO_2 plumes of both the TIC and Popocatepetl volcano on the air quality of the Mexico City Metropolitan Area (MCMA). They used the values of SO_2 reported in Rivera et al. (2009) together with satellite retrievals of vertical SO_2 columns from the Ozone Monitoring Instrument (OMI). They found that during MILAGRO the volcano contributed about one tenth of the SO_2 emissions in the MCMA whereas the rest is roughly half local and half from TIC. In addition, Rivera et al. (2009) also simulated the plume from TIC with forward particle trajectories considering both the MHR and the FPRPP. They used average emissions of SO_2 obtained with a mobile mini-DOAS system. They represented each one of them with a single stack and focused on 26 March and 4 April of 2006. The model correctly captured the plume transport. The agreement of model study with column measurements supported the estimates of SO_2 and NO_2 for the TIC plume. However, all these studies do not consider explicitly the plume of elevated flares, thus the apportionment of one of the main emitters in the TIC to regional air pollution remains unknown.

The emissions from elevated flares are difficult to quantify due to the intrinsic features of their operation; such as high stacks, strong heat radiation and the shifting of flame position by the wind speed, among others (Gogolek et al., 2010). Strosher (1996) characterized the flare emissions from two medium-height oil field battery flare systems in Alberta for both hydrocarbons and sulfur compounds. A sampling system was designed and mounted for this purpose. He reports, among others, that benzene and fluorene were abundant compounds in the field flare; and that tiophenes were present for sour solution gas flares. Hydrogen sulfide content in the sour gas ranged from 10 % to 30 %. Although he reports concentrations of combustion by-products, there were no estimates of soot emission rates in his work.

ACPD
12, 15177–15225, 2012

Most estimates for regulatory purposes are based on a set of emission factors published by the United States environmental Protection Agency (EPA). However, these rely on enclosed flares burning landfill gases or on estimates of plume opacity by trained personnel (Johnson et al., 2011). Technological differences like flare designs, applications and operating conditions can introduce more uncertainty to the estimates by these factors (McEwen and Johnson, 2011). In addition, these methodologies do not handle intermediate species formed in the combustion process that are either difficult to measure or to estimate, and which contribute to air pollution, such as volatile organic compounds, sulfur compounds and nitrogen compounds principally.

Other approaches to estimate emission rates include the application of stoichiometry calculations for flares in Nigeria (Sonibare and Akeredolu, 2004; Abdulkareem et al., 2009); the development of quantification methods based on novel measurement techniques for flares in Houston and Canada (Mellqvist et al., 2010; Johnson et al., 2011), and numerical studies with Computational Fluid Dynamics (CFD) techniques to lab-scale flares (Castiñeira and Edgar, 2008; Lawal et al., 2010), and field scale flares (Galant et al., 1984). Each of these methods provides estimates of emissions by considering in their methodology the physical and chemical aspects of a flare, thus yielding more representative rates.

The present work is related to the estimation of emission rates of combustion by-products released by a sour gas flare, in order to obtain information regarding the regional impact of flaring emissions from Tula Refinery, and to further extend this methodology for nationwide flaring activities. The main objectives are: (a) to estimate mass flow rates of primary pollutants emitted by a sour gas flare with a CFD combustion model which handles the contribution of soot radiation; (b) to model the plume of flaring operations in Tula Refinery; (c) to discuss possible contribution of the plume to MILAGRO supersites; and (d) to provide complementary information for related studies in the campaign regarding Tula emissions of SO_2 and soot.

The paper is organized as follows: Sect. 2 presents the modeling procedure; Sect. 3 results and discussion, and finally the conclusions in Sect. 4.

ACPD
12, 15177–15225, 2012

2 Models description

2.1 Combustion model

The CFD toolbox OpenFOAM® (Open Field Operation And Manipulation) version 1.5 is used to simulate the combustion part of this work. It is an open source finite volume library designed for continuum mechanics applications (Kassem et al., 2011; Marzouk and Huckaby, 2010; Weller et al., 1998). It can handle unstructured polyhedral meshes. Aside from combustion applications, it includes solvers for multiphase, incompressible and compressible flows, heat transfer and electromagnetics among others (OpenFOAM 1.5 user guide). It is capable of converting meshes constructed in commercial and open source meshing software, into its native meshing format. It also includes several numerical schemes for the temporal, gradient, divergence and laplacian terms. For the post-processing, results can be visualized with ParaView, an open source visualization application (OpenFOAM 1.5 user guide).

The reactingFoam solver is used in this work to model the flame of the representative sour gas flare. It is a transient code that solves the Navier-Stokes equations. It can use detailed chemical mechanisms to model the mixed-controlled combustion (D'Errico et al., 2007). It is based on the Chalmers Partially Stirred Reactor combustion model (PaSR) (Nordin, 2001; D'Errico et al., 2007; Marzouk and Huckaby, 2010). A transport equation that handles the turbulence-chemistry interaction is used for each chemical species the model solves, together with the equations of mass, momentum and energy:

$$\frac{\partial \overline{\rho}\widetilde{Y}_j}{\partial t} + \frac{\partial}{\partial \chi_i}\left(\overline{\rho}\widetilde{u}_i\widetilde{Y}_j\right) = \frac{\partial}{\partial \chi_i}\left(\mu_{\text{eff}}\frac{\partial \widetilde{Y}_j}{\partial \chi_i}\right) + \kappa\overline{\text{RR}}_j \tag{1}$$

In Eq. (1) the bar denotes a time-averaged value whereas the tilde represents a Favre-averaged quantity. $\widetilde{Y}_j$ is the mass fraction of the j-th species, ρ is the density of the mixture and μ_{eff} is the effective dynamic viscosity.

ACPD
12, 15177–15225, 2012

The PaSR model splits the computational cell into a reacting and a no reacting zones. With this approach, mass exchange with the reaction zone drives the change in composition. The chemical source term, $\overline{\mathrm{RR}_j}$, is scaled by κ, the reactive volume fraction which takes a value from 0 to 1. It is calculated as:

$$\kappa = \frac{\tau_{\mathrm{res}} + \tau_{\mathrm{c}}}{\tau_{\mathrm{res}} + \tau_{\mathrm{c}} + \tau_{\mathrm{mix}}} \tag{2}$$

In this expression, τ_{res} is the residence time; τ_{c} is the chemical reaction time and τ_{mix} is the mixing time which depends on μ_{eff} and the turbulent dissipation rate. The reader is referred to the references for further details.

2.1.1 reactingFoam solver set-up

The flame of the flare corresponds to an unconfined non-premixed combustion under crosswind conditions. The computational domain is a 2-D structured hexahedral mesh with dimensions of 1600 m wide and 500 m high. The flare is located at the center of the domain. The mesh is finer near the flare in order to refine the flame region. Imposed profiles of pressure, temperature and velocity are used as initial conditions. The velocity varied from 0 m s^{-1} at ground to 5 m s^{-1} at top boundary. This value is based on measurements conducted at Tula during MILAGRO campaign (IMP, 2006c). The left side of the domain is a Dirichlet boundary with the same values as the profiles for velocity and temperature. The bottom boundary is a non-slip wall. Right and top are open boundaries.

Currently, data of the gas stream is scarce; however we set a composition based on information provided by PEMEX. We are considering methane to represent natural gas, hydrogen sulfide, and nitrogen with mass fractions of 0.7, 0.2, and 0.1 respectively. The Glassman chemical mechanism is used to solve the combustion chemistry, since it considers reactions of post-combustion gases (Glassmann, 2008). It considers 83 species and 512 elementary reactions organized in 11 mechanisms, which includes the formation of both sulfur and nitrogen oxides.

ACPD
12, 15177–15225, 2012

Soot was calculated with the phenomenological model of Moss (Moss et al., 1995). It includes simplified terms describing the nucleation (α, γ), coagulation (β), surface growth (γ) and oxidation (R_{ox}) as they apply to the balance between transport and production of soot volume fraction, f_v, and particle number density, n, in non-premixed flames.

$$\frac{d\rho_s f_v}{dt} = \gamma n + \delta - \left(\frac{36\pi}{\rho_s{}^2}\right)^{1/3} n^{1/3} (\rho_s f_v)^{2/3} R_{ox} \quad (3)$$

$$\frac{d}{dt}\left(\frac{n}{N_o}\right) = \alpha - \beta \left(\frac{n}{N_o}\right)^2 \quad (4)$$

where ρ_s denotes soot particulate density and N_o is the Avogadro's number. The reader is referred to the references for further details regarding the expressions of the reaction rates, parameters and derivation.

In this work, acetylene is taken as the nucleation specie, since the nucleation rate of the model is assumed to be in proportion to the local concentration of acetylene (Brookes and Moss, 1999). Flame radiation is calculated with the P1 model (Sazhin et al., 1996; Morvan et al., 1998). The In-Situ Adaptive Tabulation (ISAT) (Pope, 1997), as implemented by D'Errico et al. (2007), is used to speed up the computing time. The mass flow of the pollutants was estimated with a slice method (see Sect. 3). The criterion for placing the slice was to consider low values of the OH radical in order to represent far-field conditions.

A representative simulation for a flare was performed; the results obtained in conjunction with the air quality model are used to further refine the combustion model. A paper dealing with this regard is under preparation (Almanza and Sosa, 2012).

2.2 Air quality model

WRF-Chem version 3.2.1 is used for the air quality simulation. It is a chemistry model fully coupled to the Weather Research and Forecasting (WRF) model (Skamarock,

ACPD
12, 15177–15225, 2012

2005) developed at the National Oceanic and Atmospheric Administration (NOAA) (Grell et al., 2005). It preserves the transport, grid and physics schemes of the meteorological component when solving the transport in sub-grid scales. Aside from the chemistry, it includes different aerosol and photolysis schemes.

2.2.1 WRF-Chem set-up

A 6-day simulation period, from 00:00 UTC 22 March to 00:00 UTC 27 March of 2006 was conducted using three domains in one-way nesting configuration. It started at 00:00 UTC on 20 March with two days of spin-up. The grid cell sizes for the domains are 27, 9 and 3 km each with 100 × 100 nodes with 35 vertical levels (Fig. 1a). The parameterizations used in this work include the Purdue Lin microphysics (Lin et al., 1983; Chen and Sun, 2002), the NOAH Land Surface Model (Chen and Dudhia, 2001), the Yonsei University (YSU) scheme for the Planetary Boundary Layer (PBL) (Hong et al., 2006), the Monin-Obukov model for the surface layer (Skamarock et al., 2005), the RRTM (Mlawer et al., 1997) and Dudhia (Dudhia, 1989) schemes for the longwave and shortwave radiation respectively. The gravity wave drag option is used for the first domain only. Six hourly Global Final Analysis data with 1° resolution were used for initial and lateral boundary conditions.

Four-dimensional data assimilation (FDDA) (Stauffer and Seaman, 1990) was used to nudge meteorology during the first 24 h of the simulation period. Only analysis nudging was applied for the first two domains. After sensitivity tests (not shown) we found it is better to turn off nudging in the PBL and in the lower ten levels as well, for wind, temperature and water vapor mixing ratio.

The model was run in concurrent mode for the first two domains with the chemistry turned off in order to save computing time. In this step we used the Grell-Devenyi scheme for the convective parameterization (Grell and Devenyi, 2002). The results for the second domain were used for boundary and initial conditions in an hourly basis for the third domain. The chemistry of the plume was solved in the third domain.

ACPD
12, 15177–15225, 2012

WRF-Chem was run with the Regional Acid Deposition Model version 2 (RADM2) chemical mechanism (Stockwell et al., 1990; Chang et al., 1989) for the gas phase and the Modal Aerosol dynamics for Europe coupled with the Secondary Organic Aerosol Model (MADE/SORGAM) mechanism for the aerosol phase (Ackermann et al., 1998; Schell et al., 2001), together with the FAST-J (Wild et al., 2000) photolysis scheme. Cumulus parameterization was turned off following the work of Zhang et al. (2009), Doran et al. (2008), and Li et al. (2010). The initial and boundary conditions are the default values computed by the model. Zhang and Dubey (2009), report small sensitivity of forecast concentrations using the default profiles. Plume rise of the flaring plume was calculated as suggested in Beychok (1995), which considers the flame length and assumes a tilted flame by 45°.

Since we are focusing only on the flaring emissions in this study, we did not use the national emission inventory; therefore no other emission was set for WRF-Chem.

3 Results and discussion

3.1 Combustion model

3.1.1 Sour Gas Flare

The results of the 2-D simulation of the sour gas flare in a cross wind are presented in Fig. 2 and Table 1. The table shows mass flow estimates of different species at five slices. These slices are located at different heights with respect to the tip of the simulated flame. The mass flow was computed with 500 points of the mixture density, velocity and species mass fraction average fields. These points were sampled for each slice at intervals of 0.1 s, for the last 6 s of simulation time (Fig. 2).

The mass flow was calculated with two approaches. In the first one (E1), the product of density and mass fraction with the velocity was done in a point-by-point basis along the slice. It considered the direction of the velocity vector in each point in order to

ACPD
12, 15177–15225, 2012

account for the inflow through the slice. The resulting profile was integrated numerically and as a result, the contribution in each of the four quadrants was computed. The mass rate was calculated by the difference between the inflow and outflow along the slice.

The second approach (E2) considered the average magnitude and average direction of the velocity along the slice. Since the number of inflow regions was small, this did not change significantly the average values of direction, which always were in the first quadrant. For each time interval the product of the profiles between density and mass fraction was multiplied with these average values and then numerically integrated. The final mass flow for both approaches was obtained with the arithmetic mean of all the calculated values at each time interval for the last six seconds of simulation time.

Our results indicate that the variation of the mass flow rate depends on the location of the slice. For this work we are interested in the region far from the flame in order to represent the conditions of the measurements by Rivera et al. (2009), which considered the plume downwind of the point sources. OH levels are estimated to infer about the region in which flaring soot is in far-field conditions. As shown in Table 1, at 30 m from the flame, OH and soot levels are relatively comparable in magnitude. At 38 m, soot levels are higher than those of OH but still comparable in magnitude. At 60 m above the flame, we considered that the influence of the atmospheric chemistry could be important, since the levels are two orders of magnitude higher than those for OH, and possibly that soot can be oxidized in the atmosphere. In addition, at this distance NO_2 levels are about two times those of NO. This can support the assumption of far flame conditions, since NO_2 concentration increases at lower temperatures. However, the levels of both SO_2 and CO_2 are more variable suggesting an increase in the domain height and hence a longer simulation time.

Nevertheless, the combustion chemical mechanism is more accurate at high temperatures, so that inherent inaccuracies are present in the estimates in the far flame regions, mainly related with the cooling of species as they are transported.

ACPD
12, 15177–15225, 2012

3.1.2 Emission rates of primary species

The estimates of mass flow rates for flaring emissions obtained with the combustion model are presented in Table 2. It shows the rates at far field conditions for the following species: SO_2, NO_x, VOCs, soot, CO_2 and CO. The rates were obtained with the two approaches discussed in the previous section. The table lists information of an emission inventory IMPei conducted by the IMP in the TIC (IMP 2006a, b), as well as the measurements by Rivera et al. (2009). Since the IMPei does not contain information of all species for the three flares, the estimated total mass flow rate is available only for SO_2, soot and CO_2.

The high variability in the stream composition of each flare can be shown with the IMPei. For SO_2 and CO_2 it is clear that sulfur and carbon are not present in a comparable quantity in all flares. This is reflected in the amount of emitted particles. Roughly, there is an order of magnitude between F1 and F3. Currently the $PM_{2.5}$ estimate of IMPei is used to compare the modeled soot estimate. The variations in the composition stream can be attributed to the Refinery configuration, since each flare is related to specific operation plants. Unfortunately there are no measurements in this respect.

SO_2 mass flow rates obtained with the combustion model are higher than the IMPei estimate for F1. IMPei roughly suggests that SO_2 emitted from F2 is half of F1, and that F3 emits about a gram. With this information the estimate for the three flares ranges from 2.91 $kg\,s^{-1}$ to 4.03 $kg\,s^{-1}$. This represents a difference of 0.97 $kg\,s^{-1}$ and 2.15 $kg\,s^{-1}$ with respect to IMPei. The range of the estimates is related to the approach used to compute the mass flow.

On the other hand, the estimates are comparable with the RdF reported value. The rates of this work are in agreement with the confidence interval of the measurements; however, the rate with E1 approach is relatively high. It is similar to the average value of the RdF estimate, which includes all the emission sources in TIC, including FPRPP.

Even though the rates obtained with the combustion model are high, these can be considered representative for Tula Refinery. For instance, Rivera et al. (2009) reports

ACPD
12, 15177–15225, 2012

high variability on the fluxes when acquiring measurements, and associate them to variation in emission of the sources in the region. In the case of flares, the contribution of wind is important, since it can diminish the combustion efficiency of flares, and therefore increase pollutant emissions. Perhaps this was captured in the main peak reported by Rivera et al. (2009) on 26 March of 2006 which was about 12.47 $kg\,s^{-1}$ for SO_2 at TIC. It is possible that this could be related with process variations, but at the same time, variations in the wind fields could have contributed.

This highlights the relevance of including flame-wind interaction in the estimation of emissions from flaring sources. It is possible that this interaction was not considered at all in the calculation method of the IMPei.

The results also suggest to increase simulation time and to refine the mesh downwind the combustion plume. For instance, eddies generated after the ignition of the flame are slowly dissipated. They present relatively high concentration of SO_2. This promotes a slower transport of these eddies by the crosswind flow. Besides, the composition and velocity of the stream sent to the flare are important, so that our assumptions also contribute to the uncertainty of the estimates. This imply to lower hydrogen sulfide concentration. In addition, the 2-D domain lacks the dynamics and flame width that can be obtained in a 3-D setup. Work is in progress to account for this in both transient and steady state.

Regarding NO_x, the estimate from this work is higher than IMPei but in agreement with RdF with respect to NO_2. The reported emission of NO_2 for the main peak of 26 March is about 0.614 $kg\,s^{-1}$ and the upper limit of RdF is 0.36 $kg\,s^{-1}$. Since IMPei reports only NO_x estimates for just one flare, it is not possible to infer which flare emits more quantity, so we assume equal values of the estimate for the three flares. For this reason, we compare with RdF estimate. The emission rate ranges from 0.14 $kg\,s^{-1}$ to 0.23 $kg\,s^{-1}$, both lower than the reported peak value and in agreement with the limits of RdF estimate. However, similar to SO_2, the rate with E1 is high.

Even though the approach of calculating the mass flow affects the results, the influence of the chemical mechanism of the combustion model is important. Currently it

ACPD
12, 15177–15225, 2012

only includes a sub-mechanism for thermal NO formation. Methane is considered to represent natural gas, so that fuel NO formation is excluded to contribute to the emissions. However, it is possible that prompt NO formation could contribute in fuel-rich conditions. In addition, the presence of sulfur in the stream complicates the dynamics in the flame because it can influence the oxidation of the fuel and affect thermal NO formation (Alzueta et al., 2001).

As for VOCs, we obtained a lower value than the IMPei estimate. Since the chemical mechanism only considers hydrocarbons up to C3, it is not possible at this stage to take into account higher hydrocarbons present in the real stream, like C4, C5 or C6 inclusive, because the computing time could be prohibitive.

Soot mass flow is lower than IMPei estimate. IMPei values suggest that F3 is 5.2 times higher than F2 and 11 times higher than F1. Considering this, our estimate is $8.01 \times 10^{-5}\,\mathrm{kg\,s^{-1}}$ for the three flares, assuming high content of elemental carbon in the IMPei particulate estimation.

Considering only methane for the fuel stream can underestimate the soot generated in the flame, since this hydrocarbon has the tendency to produce low levels of soot (Richter and Howard, 2000; Woolley et al., 2009). The Nagle-Strickland-Constable model for soot oxidation was used for R_{ox} in Eq. (3). It assumes oxidation only by O radical; however OH radical can be relevant in the oxidation step (Puri et al., 1994). Moreover, the influence of sulfur in the flame chemistry can be important in the oxidation step, since SO_3 can diminish the soot extent by generating OH radicals (Glassmann, 2008). This could influence the location of the slice in far field conditions. Thus, it is possible that the combined presence of nitrogen and sulfur affect soot formation. In addition, the original values of soot model parameters are used in this work. Moss et al. (1995) report that model parameters are sensitive to the kind of fuel in diffusion flames. In this work, perhaps the parameters are sensitive to the presence of sulfur. This is being studied in the corresponding paper (Almanza and Sosa, 2012).

Johnson et al. (2011) developed the Sky-LOSA technique, an in-situ method to quantify mass emission rates of soot from flares. They applied the method on a large-scale

ACPD
12, 15177–15225, 2012

flare at a gas plant in Uzbekistan and determined an average rate of $2\,g\,s^{-1}$ with an uncertainty of 33 %. According to Figure 1 of their paper, the flare is visibly sooty. Moreover, their estimate is representative for the overfire region of the flame. In our work, we obtained a soot emission rate on the overfire region of the simulation of 1.07 g/s, comparable in magnitude with the Sky-LOSA estimate. However, the aforementioned flare at Uzbekistan has a diameter of 1.05 m, about two times the diameter of MHR flares.

IMPei suggested emission rate is $1.07\,g\,s^{-1}$ (Table 2). Since the IMPei method does not consider the chemical interaction among species, it is possible that this estimate can be lower, because of the influence of sulfur content on soot oxidation.

CO is about 2 times higher than IMPei. With respect to the estimates at S5 slice, CO_2 is slightly lower. From the IMPei estimates, practically all the contribution is from F3. This can be attributed to the stream composition. It suggests that the gas stream of F1 and F2 can present elevated hydrogen content; however this specie was not considered in the composition of this work.

Despite the differences with reported emission rates, the estimates of this work are comparable with respect to measurements reported by Rivera et al. (2009), and IMP emissions inventory.

It is pertinent to mention that other important species for atmospheric chemistry can be calculated with the combustion model, even though they are not related with the purpose of this work. For instance, Parrish et al. (2012) report primary emissions of formaldehyde at Mont Belvieu, in the Houston Galveston Bay facilities, of $17 \pm 7\,kg\,h^{-1}$. In this work an emission rate of $11.3\,kg\,h^{-1}$ is estimated. Despite the flaring stream composition can differ at these facilities, the calculated emission is comparable in magnitude. In addition, Li et al. (2010) reports the importance of nitrous acid (HONO) in the morning photochemistry of the MCMA. In this work $0.74\,kg\,h^{-1}$ of HONO is estimated.

ACPD
12, 15177–15225, 2012

3.2 Air quality model performance

The performance of the meteorological fields obtained with WRF-chem in the third domain, is assessed by means of the Mean Absolute Error (MAE), the Root Mean Squared Error (RMSE) and the Index of Agreement (IOA) (Willmott et al., 1985; Willmot and Matsuura, 2005). The model surface variables considered for this purpose are the temperature at 2 m above ground (T), wind speed (WS) at 10 m above ground and wind direction (WD). With respect to the wind field, the RMSE of the vector wind difference (RMSEvec) is calculated. This statistic considers both speed and direction errors (Fast, 1995).

The performance was evaluated at the MCMA and at the three MILAGRO supersites. In the basin, representative monitoring stations of RAMA were selected. The surface stations were Chapingo (CHA), Cuajimpalpa (CUA), ENEP-Acatlán (EAC), Merced (MER) Plateros (PLA), Tacuba (TAC), Tlahuac (TAH), Tlalnepatla (TLA), Tlalpan (TPN), Villa de las Flores (VIF) and Xalostoc (XAL). A more detailed description of the stations can be found in (Zhang and Dubey, 2009) and (Tie et al., 2007). Results for the MCMA stations are presented in Table 3. Table 4 shows the performance at the supersites.

Surface temperature presents MAE and RMSE slightly greater than 2 °C for the considered stations, except in MER, PLA and XAL with almost 3 °C. The IOA is greater or equal than 0.9 in all stations, except in XAL where it is 0.88. In a similar way, wind speed presents MAE and RMSE close to 2 m s^{-1} in all stations, except in TPN where it is 2.20 m s^{-1} and 2.72 m s^{-1} respectively. The IOA for TPN, VIF and XAL of 0.53, 0.69 and 0.70 respectively, suggests that the model is not capturing the dynamics with enough accuracy, particularly at TPN. In this sense, the RMSEvec is also higher at TPN with 3.93 m s^{-1}. In general RMSEvec range from 2 to 3 m s^{-1} in all but CHA, TAH and TPN where is highest as previously mentioned. Although the IOA for wind direction is rather low in some of the stations, especially at TAH with 0.54, it is greater than 0.7 and less than 0.86 in most of them. However, the values of RMSE for temperature and wind speed are comparable with those reported by Zhang and Dubey (2009). In addition, the

ACPD
12, 15177–15225, 2012

highest RMSE these authors report corresponds for wind speed at TPN with a value of 2.68 m s^{-1}. According to these authors the correlation coefficient for wind direction at TPN was higher than at TAH. In this work a similar behavior of the IOA for the same stations is obtained. Nevertheless, they modeled the whole MILAGRO period and this work focuses only after 22 March as mentioned in Sect. 2.2.1.

Fast et al. (2009) report reasonable predictions of the wind fields at CHA station for the period from 6 March to 30 March. They used FDDA with observation nudging. In our work the IOA for wind speed and direction is relatively high for this station. They also had inaccuracies at XAL and VIF because the model tended to over-predict the extent of the gap flow. Moreover, the downslope flows in their simulation not propagated at night in stations near the western side of the basin rim, except in CUA. Similar behavior is obtained in our work at TAC and TAH with low IOA for wind direction and at CUA with a moderately IOA for wind direction.

On the other hand, the model captured relatively well the dynamics of temperature at the three supersites, with slightly better performance at T0. The MAE is less than 2 °C and the IOA is greater than 0.9 in all the sites. The model better captured wind speed behavior at T0, with both MAE and RMSE about 1 m s^{-1}, and with an IOA of 0.82. For the other sites, the performance was slightly better at T2 with an IOA of 0.76 and a MAE less than 2 m s^{-1}. With respect to the IOA, the model resolved wind direction more accurately at T2. This value is very similar to T1 with 0.81. However, at T0 the model apparently had the lowest performance. Nevertheless, the RMSEvec is 2.61 m s^{-1} and lower than those of T1 and T2.

Aside from the inherent variability in the parameterizations employed by WRF, possible reasons for the inaccuracy in the performance of the model can be attributed to the vertical resolution of the grid, since the first level in this work is located about 50 m above surface. In this respect, Zhang et al. (2009) seems to place the first level below 50 m since their higher resolution within the boundary layer is around 10 to 100 m. This can give higher wind speeds with respect to surface observations since the height of the monitoring equipment is even less than the first mass level of the model. Nevertheless,

ACPD
12, 15177–15225, 2012

Li et al. (2010), also place the first level of the model at around 50 m without visible impact in the performance of their simulations. Moreover, the local topographic and thermal effects are not well captured (Doran et al., 2009) and can influence the modeled wind direction at the surface. In addition, de Foy et al. (2009b) employ high resolution satellite remote sensing data for the land surface model and without data assimilation to improve the model performance. It is worth to mention that the simulation period in our work covers the last two cold surge events (NORTE2 and NORTE3) described in (Fast et al., 2007). These add more variability to the dynamics of the simulation period. Since no convective parameterization was included for the innermost domain in this work, this could have contributed to the accuracy of the model as well. De Foy et al. (2009b) turned it on, whereas Zhang and Dubey (2009), Zhang et al. (2009), Li et al. (2010) and Doran et al. (2008) turned it off, but in the latter study observations were assimilated into the model as previously mentioned.

Although the statistics suggest improvement in the model set-up, the meteorological fields can be considered reliable for this study given the moderately high values of IOA for the surface wind field together with the performance of surface temperature.

3.3 Flaring plume transport

This section presents the WRF-Chem simulations of the plume by flaring activities at Tula Refinery (Fig. 1b). Only the estimates of SO_2, soot, NO_x, CO, C_2H_2 and C_2H_4 are considered as inputs to WRF-Chem. The latter two hydrocarbons were considered since acetylene is important to soot formation and ethylene is an important by-product in methane rich combustion (Law, 2006). Table 5 presents the mass rates considered for inputs to WRF-Chem.

For NO_x the same estimate of NO_2 and NO was used for F3, and considered 30 % less for F1 and F2. This ensures the values to be in agreement with measurements. For soot the same value of the estimate was set equally for the three flares. With CO, 30 % less for F1 and F2 was considered, similar to NO_x. As with soot, the estimates

ACPD
12, 15177–15225, 2012

of both C_2H_2 and C_2H_4 are equal for the three flares. All of the emissions are held constant in all the simulation period.

3.3.1 SO_2

Given the overestimation obtained with the combustion model, it was decided to constrain the total emission rate of SO_2 for the three flares. This was accomplished by setting the emission rate to roughly $3\,kg\,s^{-1}$. This allows the emission rate to be in relative agreement with measurements without losing generality with the combustion model. Surface measurements of SO_2 at T0 and T1 are used to compare the results of the model (Fig. 3).

At T0, the model suggests a contribution after midnight on 22 March until 05:00 LT. There was a northerly wind on the previous day that transported the plume at this site, with a strong lateral transport from the east after midnight. Measurements show a second peak that also started at 05:00 LT. It is related with local sources since the wind fields show a southerly component that transported the plume to the north so that the entire plume left T0 early on this day. On 23 March northerly winds prevailed most of the day, and the plume reached T0 again in the early morning. The model captured the gradual increase of the observations after 02:00 and until 07:00, with a small decrease after this hour. However, there were missing data in this period to confirm it, but the results suggest that it is related with topographic effects of Sierra de Guadalupe together with stability conditions. As the plume was further transported by the northwesterly component, the model captured the evolution along the day as showed by the observations. Although the timing of the peak was slightly underpredicted, nudging was important to capture relatively well the phase of the observations peaks, reflecting in a more accurate timing. According to the model, the greatest contribution in SO_2 levels by the plume of TIC occurred on this day. It is important to mention that the plume practically spent most of the day in the basin.

On 24 March, a northeasterly component prevented the plume to be transported to the basin and practically there was no contribution at T0. The model suggests that the

ACPD
12, 15177–15225, 2012

small peak at 19:00 is originated by downslope flow that promoted the recirculation of a residual mass of the plume located at the western side of the basin. However, the measurements show two peaks along the day with higher concentration than on 23 March, from 08:00 to 21:00 LT. A peak was measured at T1 with a similar timing to the first peak at T0. It is possible that this was a contribution from Tula, since on 23 March peaks with a similar evolution were registered at both T0 and T1 (Fig. 3). Nevertheless the model did not capture this since the plume moved farther to the west without reaching the basin. De Foy et al. (2009a) attributed this to subtle changes in the strength of the down-valley flow from the northeast, and the up-valley flow to Tula also from the northeast, which totally change the resulting plume transport.

The recirculation was present in the early morning of 25 March until a northerly flow gradually transported the plume back to the basin. The model suggests that the plume reached T0 after midday. Observations show no clear peak after midday, but the model is in relative agreement with the dynamics of the measurements for the rest of this day. 26 March presents a similar behavior, with the contribution mostly by recirculation before midday and with a late northerly flow in the afternoon. Nevertheless, the levels of SO_2 at night are lower than on 25 March, because a southerly component removed most of the plume before midnight. However, winds from the northwest and later form the northeast transported the plume back to the basin, so that recirculation was important for SO_2 levels at T0 on this day.

This mechanism was also important in early hours of 27 March. At these hours, nearby Tula, there was flow from both the southeast and southwest that transported the plume further to the north, supporting the increment of emissions by recirculation. The gradual decrease of SO_2 levels as shown by observations is correctly captured by the model.

At T1 the behavior is similar in all the simulation period. The main difference is related to the influence of local sources on SO_2 levels, since the diurnal cycle is not as visible as at T0. Nevertheless, measured values are about two times greater than at T0. On

ACPD
12, 15177–15225, 2012

23 and 25 March the model captured the transport of the plume first reaching T1 and then T0. This reflects in the timing of the peaks in the observations.

In order to infer about the influence of the emission rate on the modeled concentration values at the supersites, a similar simulation was conducted by lowering the emission rate of SO_2 to 1.97 kg s^{-1} for the three flares. It corresponds to the rate obtained with E2, in agreement with both IMPei and RdF, and was assumed that most of the contribution is from flare F1. Results suggest maximum differences for 23 March, particularly in the afternoon, of about 4 ppb at T0 and 27 ppb at T1. The peak for this day was also reproduced as in the previous simulation, and in general the same behavior was obtained for the time series. For the other days the maximum differences are 7 ppb at T0 and 8 ppb at T1. These values suggest that even though the estimate of SO_2 obtained with the combustion model is high, the differences in concentration levels are relatively low in the whole simulation period at both supersites. The relatively high difference at T1 on 23 March can be attributed to variations in the wind fields and topographic effects.

With these two scenarios, the average contribution of flaring emissions from MHR to the total SO_2 levels was calculated for the simulation period. Results are presented in Table 6. When using the higher emission rate estimate the contribution is about 37 % at T0 and 39 % at T1. With the lower emission estimate, the average contribution is 23 % at T0 and 29 % at T1. This yields a global difference between the two scenarios of about 14 % at T0 and 10 % at T1. The corresponding average concentration is of 2.22 ppb and 1.42 ppb at T0. At T1 a concentration of 2.02 ppb and 1.48 ppb is obtained for each emission rate.

De Foy et al. (2009a) present impact fractions in the MCMA by emissions from TIC for the whole MILAGRO campaign. They are about 40 % to 57 %, according to different configurations in their model set-up. This suggests the possibility of periods when TIC emissions can impact more than local sources. According to our results, it is possible that on 23 March, emissions from MHR contributed more than local sources to the total

ACPD
12, 15177–15225, 2012

SO_2 levels at T0. However, it is important to note that we did not include the urban emissions in this study.

3.3.2 Soot transport

Elemental carbon (EC) is considered to represent soot. Surface measurements of elemental carbon at the three supersites obtained during the MILAGRO campaign (Molina et al., 2010) were used to compare model results. Although soot is transported together with SO_2 and other species, the time series between these species present differences in the local dynamics. The meteorological fields are similar for both species so that part of the discussion of SO_2 applies for soot.

The predicted concentrations of EC at T1 are compared with observations in Fig. 4. It can be noted that the modeled concentration is about three orders of magnitude lower than observations. Aside from the inherent uncertainty of the estimate, one possible reason for such a difference can be attributed to the influence of local sources.

Another simulation was conducted using estimates of $PM_{2.5}$ obtained by the IMP (IMP, 2006b). The emission rate considered all the possible combustion sources for MHR and FPRPP. The purpose to include other sources of soot rather than just elevated flares is to determine if dilution is relevant. The mass rate was set to $0.23\,kg\,s^{-1}$ for both FPRPP and MHR. Similar to de Foy et al. (2009a), we set one stack for FPRPP and used the three stacks for the flares to represent all the MHR emissions. Results are shown in Fig. 5.

Because we did not include the national emission inventory, the diurnal variation at T0 and T1 is not captured. Instead, the modeled time series reveals the days with most possible contribution from TIC in EC levels at the three sites. According to the model, there were small contributions after midnight in all the sites on 22 March. In contrast, after 24 March, most of the contributions possibly occurred late in the morning and early in the afternoon.

At T0 it is evident the influence of local sources, since the maximum modeled concentration is comparable to low background levels. Fast et al. (2009) show in panel (d)

ACPD
12, 15177–15225, 2012

of Fig. 1 in their paper biomass burning sources close to T0. However, after 23 March the frequency and intensity of fires diminished considerably with the NORTE3 (Fast et al., 2007).

At T1 a similar contribution of local sources is also present, but with lower magnitude. For instance, the emissions from the highway connecting Mexico City and Pachuca can be important (Fast et al., 2007). Because T2 is a remote site, daily variations are more frequent so that diurnal patterns are not as pronounced as in the other sites, and dilute plumes from nearby sources are more important (Fast et al., 2009). This implies that a contribution of the plume from TIC could present a similar timing with the peak of EC observations at this site. Thus, the influence of local sources at T0 and T1 can induce a difference in the timings between the plume of TIC and the peaks from observations. For instance, on 22 March the main peak of observations at T0 is at about 06:00 LT, while the model peak is around midnight.

This can be observed with more clarity on 23 March. On this day the model suggests a transport from T2 to T1 to T0. At T2 the observations show that after 04:00, a peak started to develop and ended at 13:00. The model captured this peak, its gradual diminishing, and the timing of the maximum value at 05:00 LST. However, the concentration value was overpredicted and the peak ended earlier, at about 11:00.

As the plume continued to be transported, it reached T1 at 09:00. In the early morning, the surface fields suggest that southerly wind was present at T1 with a gradual flow developing from the north later in the morning. In contrast, the observed peak was at 06:00. Therefore, it is possible that the peak of the observations can be related to local sources, and that TIC emissions were more important before midday.

The plume reached T0 at 10:00, with the peak at 11:00. As at T1, there was southerly flow at this site in the early morning with slope flow from the western side of the basin. In the model, however, the slope flow is moderately captured near the NW side of the basin, since the IOA for wind direction is around 0.7 for EAC, TAC, and TLA (Table 1). The gradual decrease in the observations from 08:00 can be attributed to northerly flow. The peak from the plume coincides roughly with the minimum of the observations,

ACPD
12, 15177–15225, 2012

suggesting that around midday of 23 March part of the EC levels at T0 came from TIC. Similar to the discussion of SO_2 time series, it is possible that on 24 March a contribution form Tula was not captured by the model.

The model shows that the plume impacted the three sites on 25 March and 26 March. The behavior is similar on 25 March at T2, with the peak from the model and observations at 09:00. However at T1 the model suggest a peak at midday, but the observations indicate small values at that hour. It is possible that the timing of the plume was not correctly captured and the possible contribution occurred earlier. Nevertheless, at T0 the model peak coincides with the minimum of the observations at 14:00, similar to 23 March. Local sources could contribute to the peaks before the plume reached the sites.

On 26 March the model suggests a contribution from early morning until midday at T1. Later at T2, the timing of the model peak agrees with the observations at 14:00. In this case, most of the modeled levels of EC at this site are due to a recirculation as discussed for SO_2. In contrast, the plume directly impacts T1 first and later T0. The observations minimum value at T0 is close to the model maximum, like on 23 March. According to calendar, this day corresponds to Sunday. This reflects in the time series since there were no sharp peaks in the morning. The influence of local sources at T0 and T1 are clearer on this day. On 27 March, there was a slight contribution at T1 in the morning; at T2 after midday, and no visible contribution at T0 before 17:00.

Fast et al. (2009), report considerable underestimation of EC at T0 and T1 in the period from 05:00 to 10:00. In our work, the model suggests contribution by TIC at T1 in the period after 05:00 until 10:00 inclusive, on 23, 25, 26, and 27 March. Nevertheless, it was clearer on 23 March. However, since at this stage the model is not considering aqueous reactions, possible scavenging by precipitation on rainy days as suggested by Doran et al. (2008), can be relevant.

Although the plume can dilute as it is transported, EC levels are comparable in order of magnitude when taking into account all the combustion sources at TIC. For this reason, if we take the IMP estimate for flares and compare it with the total of TIC, it implies

ACPD
12, 15177–15225, 2012

that it is about 68 times lower. This suggests that low values of EC, obtained with the combustion model emission rate estimate, are feasible and thus the contribution of local sources is rather more important.

As with SO_2 the contribution of flaring activities at TIC to the total soot levels was estimated. In order to complement the contribution estimation another simulation was performed by means of taking the mass rate at the overfire region of the flame. This corresponds to slice S0 in Table 1. Results are presented in Table 6.

When considering the total emissions of the power plant and the refinery, more than half of the total levels at T2 can be attributed to TIC in the simulation period, and less than 10 % at T0. At T1, the contribution is roughly double of T0 in all scenarios. The influence of the slice location for estimating the soot mass flow rate is about an order of magnitude higher when taking the overfire region, than when considering the far flame region. These results support the importance of local sources on predicting soot concentration levels.

Figure 6 presents the plume from TIC on 23 March at 12:00, for the considered air pollutants. It shows the transport of the plume under the influence of complex meteorology.

A contribution plot was constructed in order to infer about the possible surface impact of the TIC flaring plume. An area encompassing most of the Tula region and the basin was selected. It was performed by taking a threshold value for each pollutant, which is based on the detection limits of the measuring instruments. We set 0.01 $\mu g\,m^{-3}$ for soot and 1 ppb for SO_2. Then we count the number of hours in which this threshold was exceeded in all the simulation period. The plot is shown in Fig. 7.

The figure shows the time, as percent of hours for the simulation period, that the flaring plume spent in representative locations within this region. The considered scenarios for soot are the overfire rate and the FPRPP+MHR emissions. For SO_2 we took the rates obtained with E1 and E2 approach of the slice method.

The spatial distribution is similar to that reported by Zambrano García et al. (2009), with a tendency of transport towards the northeast. It can be noted that for primary

ACPD
12, 15177–15225, 2012

pollutants the distribution is similar, but it can change for secondary pollutants. The plot suggests that the plume spent more time at T0 than at the other supersites. This implies that the north region of the basin was the most exposed to emissions from flaring operations. However, when considering the soot emissions of FPRPP and MHR, the plume can spread farther to the south of the basin for this simulation period. SO_2 presents a similar behavior.

Since the flares operate continuously, there exists the potential of a constant exposure, even though the concentration is small. These contribution plots can give further information when considering the emission inventory, and may provide supporting information for exposure in specific regions which can include vegetation, crops, soils and population.

4 Conclusions

This work presents simulations of the plume emitted by the three elevated flares of Tula Miguel Hidalgo Refinery, in order to study the contribution of flaring emissions at the MILAGRO supersites. This was accomplished by calculating mass flow rates of combustion by-products with OpenFOAM®, and further input them to WRF-Chem. The emission rates of primary pollutants were estimated for a representative sour gas flare in a 2-D configuration. The model allows the quantification of species relevant for atmospheric chemistry. The mass flow was obtained with a slice method. In particular, C_2H_2, C_2H_4, NO_x, SO_2, CO and soot were obtained with the combustion model. This model takes into account the cross wind interaction with the flame and the content of hydrogen sulfide, important aspects not considered at all by emission factors methodologies.

Several slices were placed at different locations with respect to the tip of the flame. When considering the far flame slice, soot emission is about $60\,mg\,s^{-1}$ compared to $2.63\,g\,s^{-1}$ of the emission factor by the IMP. However, when taking the overfire slice, it yielded a rate of about $1\,g\,s^{-1}$, which is of the same magnitude. Moreover, the overfire

ACPD
12, 15177–15225, 2012

estimate was comparable to the Sky-LOSA estimate of a large-scale flare by Johnson et al. (2011). As for SO_2, the difference with the IMP emission factor ranged from $0.6\,kg\,s^{-1}$ to $1.4\,kg\,s^{-1}$ according to the estimation method (E1 or E2).

On the other hand, the emission rates for SO_2 and NO_2 are in the range of estimates obtained with measurements during the MILAGRO campaign by Rivera et al. (2009). For SO_2 the highest calculated rate of this work is $2.73\,kg\,s^{-1}$, which is within the range of $4.90 \pm 3.80\,kg\,s^{-1}$ by the measurements. The calculated rate for NO_2 is $6.88 \times 10^{-2}\,kg\,s^{-1}$ and the measurements suggest $2.77 \times 10^{-1} \pm 8.10 \times 10^{-2}\,kg\,s^{-1}$.

The impact of these emissions on the air quality of MILAGRO supersites was further evaluated for the period from 22 March to 27 March of 2006, focusing on SO_2 and soot. Given the relatively good values of MAE, RMSE, RMSEvec and IOA, the performance of WRF-Chem was reliable enough to compare results with surface measurements at MILAGRO supersites. Analysis nudging was important to capture relatively well the timing when the plume reached the three supersites, given the relative agreement of model peaks with observation peaks in some days of the simulation period. However, further improvement is recommended, particularly the refinement of the vertical levels within the PBL, to consider convective parameterization in the inner domain and perhaps to perform warm starts for periods of days instead of a continuous run.

The results from the present study suggest a more feasible contribution of TIC in SO_2 levels on 23 March in most of the basin, with similar behavior on 25 March of 2006, and with a potential contribution on 24 March according to measurements The estimated contribution of elevated flares to total SO_2 levels is about 37 % at T0 and 39 % at T1. The high contribution values can be attributed to the persistence of the plume in the basin on 23 March.This information can support related studies regarding the possible recovery of the gas in the refinery.

These results complement previous findings of studies related to TIC conducted by other research groups, and at the same time it gives the possibility to extend this study to infer about the contribution of flaring activities to levels of secondary pollutants in the MCMA and near the refinery.

ACPD
12, 15177–15225, 2012

As for soot, the model suggests that the flaring plume has less influence at the supersites, compared to local sources. Concentration values of EC less than 1 $\mu g\,m^{-3}$ are feasible at the supersites as well as in the basin. When all the combustion sources of FPRPP and MHR were considered into the model, the contribution of local sources remained, so that background concentration was higher than model concentrations in almost all the simulation period. Since the national emission inventory was not included, this could have contributed to the difference between observed and modeled concentration of soot. Even though results suggest flare emissions are not significant for urban locations near the MCMA, they can exert a greater contribution to both urban and rural areas near the refinery.

Results showed a transport of emissions from T2 to T1 to T0 on 23 March, when meteorology favored northeasterly winds due to the presence of the third cold surge. At T2 the model peaks agrees relatively well with observations.

The estimated contribution of flares to total soot levels is sensitive to the location of the slice in the combustion model. As stated above, overfire estimate led to better agreement with IMP emission factors and this resulted in a suggested contribution of 0.14 % at T0, 0.3 % at T1, and 1.02 % at T2. Nevertheless, when considering all the possible emission sources at TIC, including the power plant, the contribution is about 7 %, 17 % and 59 % at T0, T1 and T2 respectively.

For the simulation period of this study, the flaring plume spent more time at T0 than at the other supersites. This implies that the north region of the basin can have more exposure to TIC pollutants, which is in agreement with previous studies. It also showed that when considering emissions of the power plant, the plume can reach part of the south region of the basin. When considering the emission inventory, secondary pollutants can be included to complete the analysis.

The combustion model requires further improvement, particularly in selecting the location of the slice and the gas stream composition. The estimates of this work can be helpful for delimiting the combustion emissions by the flares of MHR. Moreover, as a separate result, it was possible to suggest a first estimate of nitrous acid and

ACPD
12, 15177–15225, 2012

formaldehyde, a highly reactive organic compound (HRVOC), and which was of similar magnitude to the measurements by Parrish et al. (2012).

Although this work focused on Tula Refinery, it is feasible to apply these tools to a country-wide analysis of the impact of flaring activities in Mexico. For instance, it can extend the modeling of air quality emissions of offshore flares in Campeche Sound previously conducted by the IMP (Villaseñor et al., 2003).

Acknowledgements. The authors thank Tommaso Lucchini for his help with the soot code, Georg Grell for his comments regarding WRF-Chem, Ed Scott Wilson Garcia for his help with MPICH and Guohui Li for his support with WRF-Chem. In addition, the use of the experimental data of the MILAGRO campaign is greatly acknowledged.

References

Abdulkareem, A. S., Odigure, J. O., and Abenge, S.,: Predictive model for pollutant dispersion from gas flaring: a case study of oil producing area of Nigeria, Energ. Source. Part A, 31, 1004–1015, 2009.

Ackermann, I. J., Hass, H., Memmesheimer, M., Ebel, A., Binkowski, F. S., and Shankar, U.: Modal aerosol dynamics model for Europe: development and first applications, Atmos. Environ., 32, 2981–2999, 1998.

Almanza, V. H. and Sosa, G.: Numerical estimation of the emissions of an industrial flare, in preparation, 2012.

Alzueta, M. U., Bilbao, R., and Glarborg, P.: Inhibition and sensitization of fuel oxidation by SO2, Combust. Flame, 127, 2234–2251, 2001.

Beychok, M. R.: Fundamentals of Stack Gas Dispersion, Third Edition, Ch. 11, ISBN 0-9644588-0-2., 1995.

Bond, T. C., Zarzycki, C., Flanner, M. G., and Koch, D. M.: Quantifying immediate radiative forcing by black carbon and organic matter with the Specific Forcing Pulse, Atmos. Chem. Phys., 11, 1505–1525, doi:10.5194/acp-11-1505-2011, 2011.

Brookes, S. J. and Moss, J. B.: Predictions of soot anf thermal radiation properties in confined turbulent jet diffusion flames, Combust. Flame, 116, 486–503, 1999.

ACPD

12, 15177–15225, 2012

Castiñeira, D. and Edgar T.: Computational Fluid Dynamics for simulation of crosswind on the efficiency of high momentum jet turbulent combustion flames, J. Environ. Eng., 134, 561–571, 2008.

Chen, F. and Dudhia, J.: Coupling an advanced land-surface/hydrology model with the Penn State/NCARMM5modelingsystem. Part I: Model description and implementation, Mon. Weather Rev., 129, 569–585, 2001.

Chen, S. H. and Sun, W. Y.: A one-dimensional time dependent cloud model, J. Meteorol. Soc. Jpn., 80, 99–118, 2002.

Cifuentes, E., Blumenthal, U., Ruíz-Palacios, G., Bennett, S., and Peasey, A.: Epidemiological panorama for the agricultural use of wastewater: The Mezquital Valley, Mexico, Salud Publica Mexico, 36, 3–9, 1994.

de Foy, B., Varela, J. R., Molina, L. T., and Molina, M. J.: Rapid ventilation of the Mexico City basin and regional fate of the urban plume, Atmos. Chem. Phys., 6, 2321–2335, doi:10.5194/acp-6-2321-2006, 2006.

de Foy, B., Krotkov, N. A., Bei, N., Herndon, S. C., Huey, L. G., Martínez, A.-P., Ruiz-Suárez, L. G., Wood, E. C., Zavala, M., and Molina, L. T.: Hit from both sides: tracking industrial and volcanic plumes in Mexico City with surface measurements and OMI SO2 retrievals during the MILAGRO field campaign, Atmos. Chem. Phys., 9, 9599–9617, doi:10.5194/acp-9-9599-2009, 2009a.

de Foy, B., Zavala, M., Bei, N., and Molina, L. T.: Evaluation of WRF mesoscale simulations and particle trajectory analysis for the MILAGRO field campaign, Atmos. Chem. Phys., 9, 4419–4438, doi:10.5194/acp-9-4419-2009, 2009b.

D'Errico, G., Ettorre, D., and Lucchini T.: Comparison of combustion and pollutant emission models for DI Engines, SAE paper, 2007-24-005, 2007.

Doran, J. C., Fast, J. D., Barnard, J. C., Laskin, A., Desyaterik, Y., and Gilles, M. K.: Applications of lagrangian dispersion modeling to the analysis of changes in the specific absorption of elemental carbon, Atmos. Chem. Phys., 8, 1377–1389, doi:10.5194/acp-8-1377-2008, 2008.

Dudhia, J.: Numerical study of convection observed during the winter monsoon experiment using a mesoscale two-dimensional model, J. Atmos. Sci., 46, 3077–3107, 1989.

Fast, J. D.: Mesoscale modeling and four-dimensional data assimilation in areas of highly complex terrain, J. Appl. Meteorol., 34, 2762–2782, 1995.

Fast, J. D., de Foy, B., Acevedo Rosas, F., Caetano, E., Carmichael, G., Emmons, L., McKenna, D., Mena, M., Skamarock, W., Tie, X., Coulter, R. L., Barnard, J. C., Wiedinmyer, C., and

ACPD
12, 15177–15225, 2012

Madronich, S.: A meteorological overview of the MILAGRO field campaigns, Atmos. Chem. Phys., 7, 2233–2257, doi:10.5194/acp-7-2233-2007, 2007.
Fast, J., Aiken, A. C., Allan, J., Alexander, L., Campos, T., Canagaratna, M. R., Chapman, E., DeCarlo, P. F., de Foy, B., Gaffney, J., de Gouw, J., Doran, J. C., Emmons, L., Hodzic, A., Herndon, S. C., Huey, G., Jayne, J. T., Jimenez, J. L., Kleinman, L., Kuster, W., Marley, N., Russell, L., Ochoa, C., Onasch, T. B., Pekour, M., Song, C., Ulbrich, I. M., Warneke, C., Welsh-Bon, D., Wiedinmyer, C., Worsnop, D. R., Yu, X.-Y., and Zaveri, R.: Evaluating simulated primary anthropogenic and biomass burning organic aerosols during MILAGRO: implications for assessing treatments of secondary organic aerosols, Atmos. Chem. Phys., 9, 6191–6215, doi:10.5194/acp-9-6191-2009, 2009.
Galant, S., Grouset, D., Martinez, G., Micheau, P., and Allemand J. B.: Three-dimensional steady parabolic calculations of large scale methane turbulent diffusion flames to predict flame radiation under cross-wind conditions, Twentieth Symposium International on Combustion, 531–540, 1984.
General Electric Energy, Flare Gas Reduction, Recent global trends and policy considerations, available at: http://www.ge-energy.com/content/multimedia/_files/downloads/GE%20Flare%20Gas%20Reduction%2001-24-2011.pdf, 2011, last access: June 2012.
Glassman, I. and Yetter, R. A.: Combustion, 4th Edition, Academic Press, 2008.
Gogolek, P., Caverly, A., Schwartz, R., and Pohl, J.: Emissions from elevated flares – a survey of the literature, Report for the International Flaring Consortium, Canada, 2010.
Grell, G. A., Peckham, S. E., Schmitz, R., McKeen, S. A., Frost, G., Skamarock, W. C., and Eder, B.: Fully coupled "online" chemistry within the WRF model, Atmos. Environ., 39, 6957–6975, 2005.
Grell, G. A. and Devenyi, D.: A generalized approach to parameterizing convection combining ensemble and data assimilation techniques, Geophys. Res. Lett., 29, 1693, doi:10.1029/2002GL015311, 2002.
Hong, S.-Y., Noh, Y. and Dudhia, J.: A new vertical diffusion package with an explicit treatment of entrainment processes, Mon. Weather Rev., 134, 2318–2341, 2006.
IMP: Estudio de las emisiones de la zona industrial de Tula y su impacto en la calidad del aire regional, IMP, PS-MA-IF-F21393-1, 2006a.
IMP: Estudio de las emisiones de la zona industrial de Tula y su impacto en la calidad del aire regional, IMP, PS-MA-IF-F21393-1, Anexo C, 2006b.

ACPD
12, 15177–15225, 2012

IMP: Estudio de las emisiones de la zona industrial de Tula y su impacto en la calidad del aire regional, IMP, PS-MA-IF-F21393-1, Anexo E, 2006c.
Johnson, M., Devillers, R. W. and Thomson K. A.: Quantitative field measurement of soot emission from a large gas flare using Sky-LOSA, Environ. Sci. Technol., 45, 345–350, 2011.
Kassem, H. I., Saqr, K. M., Aly, H. S., Sies, M. M., and Wahid, M. A.: Implementation of the eddy dissipation model of turbulent non-premixed combustion in OpenFOAM, Int. Commun. Heat Mass, 38, 363–367, 2011.
Law, C. K.: Combustion Physics, Cambridge University Press, 2006.
Lawal, M. S., Fairweather, M., Ingham, D. B., Ma, L., Pourkashanian, M., and Williams, A.: Numerical study of emission characteristics of a jet flame in cross-flow, Combust. Sci. Technol., 182, 1491–1510, 2010.
Li, G., Lei, W., Zavala, M., Volkamer, R., Dusanter, S., Stevens, P., and Molina, L. T.: Impacts of HONO sources on the photochemistry in Mexico City during the MCMA-2006/MILAGO Campaign, Atmos. Chem. Phys., 10, 6551–6567, doi:10.5194/acp-10-6551-2010, 2010.
Lin, Y.-L., Farley, R. D., and Orville, H. D.: Bulk parameterization of the snow field in a cloud model, J. Appl. Meteorol., 22, 1065–1092, 1983.
Marzouk, O., Huckaby, E. D.: A comparative study of eight finite-rate chemistry kinetics for CO/H2 combustion, Eng. Appl. Comput. Fluid Mech., 4, 331–356, 2010.
McEwen, J. D. N. and Johnson, M. R.: Black Carbon Particulate Matter Emission Factors for Buoyancy Driven Associated Gas Flares, J. Air Waste Manage., 62. 307–321, doi:10.1080/10473289.2011.650040, 2012.
Mellqvist, J., Johansson, J., Samuelsson, J., Offerle, B., Rapenglück, B., Wilmot, C., and Fuller, R.: Investigation of VOC radical sources in the Houston Area by the Solar Occultation Flux (SOF) method, mobile DOAS (SOF-II) and mobile extractive FTIR, Final Report TERC Project H-102, 2010.
Mlawer, E. J., Taubman, S. J., Brown, P. D., Iacono, M. J., and Clough, S. A.: Radiative transfer for inhomogeneous atmosphere: RRTM, a validated correlated-k model for the long-wave, J. Geophys. Res., 102, 16663–16682, 1997.
Moffet, R. C. and Prather, K. A.: In-situ measurements of the mixing state and optical properties of soot with implications for radiative forcing estimates, PNAS, 106, 11872–11877, doi:10.1073/pnas.0900040106, 2009.
Molina, L. T., Madronich, S., Gaffney, J. S., Apel, E., de Foy, B., Fast, J., Ferrare, R., Herndon, S., Jimenez, J. L., Lamb, B., Osornio-Vargas, A. R., Russell, P., Schauer, J. J., Stevens, P.

ACPD
12, 15177–15225, 2012

S., Volkamer, R., and Zavala, M.: An overview of the MILAGRO 2006 Campaign: Mexico City emissions and their transport and transformation, Atmos. Chem. Phys., 10, 8697–8760, doi:10.5194/acp-10-8697-2010, 2010.
Morvan, D., Portiere, B., Larini, M., and Loraud, J. C.: Numerical simulation of turbulent diffusion flame in cross flow, Combust. Sci. Technol., 140, 93–122, 1998.
Moss, J. B., Stewart, C. D., and Young, K. J.: Modeling soot formation and burnout in a high temperature laminar diffusion flame burning under oxygen enriched combustion, Combust. Flame, 101, 491–500, 1995.
Nordin, N.: Complex chemistry modeling of diesel spray combustion, Ph.D. thesis, Chalmers University of Technology, Sweden, 55 pp., 2001.
OpenFOAM 1.5 User Guide, available from: http://www.opencfd.co.uk/openfoam/doc/user.html.
OpenFOAM: The Open Source CFD Toolbox, available from: http://www.openfoam.org
Parrish, D. D., Ryerson, T. B., Mellqvist, J., Johansson, J., Fried, A., Richter, D., Walega, J. G., Washenfelder, R. A., de Gouw, J. A., Peischl, J., Aikin, K. C., McKeen, S. A., Frost, G. J., Fehsenfeld, F. C., and Herndon, S. C.: Primary and secondary sources of formaldehyde in urban atmospheres: Houston Texas region, Atmos. Chem. Phys., 12, 3273–3288, doi:10.5194/acp-12-3273-2012, 2012.
Pope, S.: Computationally Efficient Implementation of Combustion Chemistry Using In-Situ Adaptive Tabulation, Combust. Theor. Model., 1, 41–63, 1997.
Puri, R., Santoro, R., and Smyth, K.: The oxidation of soot and carbon monoxide in hydrocarbon diffusion flames, Combust. Flame, 97, 125–144, 1994.
Querol, X., Pey, J., Minguillón, M. C., Pérez, N., Alastuey, A., Viana, M., Moreno, T., Bernabé, R. M., Blanco, S., Cárdenas, B., Vega, E., Sosa, G., Escalona, S., Ruiz, H., and Artíñano, B.: PM speciation and sources in Mexico during the MILAGRO-2006 Campaign, Atmos. Chem. Phys., 8, 111–128, doi:10.5194/acp-8-111-2008, 2008.
Richter, H. and Howard, J. B.: Formation of polycyclic aromatic hydrocarbons and their growth to soot – a review of chemical reaction pathways, Prog. Energ. Combust. Sci., 26, 565–608, 2000.
Rivera, C., Sosa, G., Wöhrnschimmel, H., de Foy, B., Johansson, M., and Galle, B.: Tula industrial complex (Mexico) emissions of SO_2 and NO_2 during the MCMA 2006 field campaign using a mobile mini-DOAS system, Atmos. Chem. Phys., 9, 6351–6361, doi:10.5194/acp-9-6351-2009, 2009.

ACPD
12, 15177–15225, 2012

Sazhin, S. S., Sazhina, E. M., Faltsi-Saravelou, O., and Wild, P.: The P-1 model for thermal radiation transfer: advantages and limitations, Fuel, 75, 289–294, 1996.
SEMARNAT-INE, Secretaria del Medio Ambiente y Recursos Naturales/Instituto Nacional de Ecologia: Inventario Nacional de Emisiones de Mexico 1999, Mexico, 2006.
Skamarock, W. C., Klemp, J. B., Dudhia, J., Gill, D. O., Barker, D. M., Wang, W., and Powers, J. G.: A description of the advanced research WRF version 2, NCAR Technical Note, NCAR/TN-468+STR, 8 pp., 2005.
Skeie, R. B., Berntsen, T., Myhre, G., Pedersen, C. A., Ström, J., Gerland, S., and Ogren, J. A.: Black carbon in the atmosphere and snow, from pre-industrial times until present, Atmos. Chem. Phys., 11, 6809–6836, doi:10.5194/acp-11-6809-2011, 2011.
Sonibare, J. A. and Akeredolu, F. A.: A theoretical prediction of non-methane gaseous emissions from natural gas combustion, Energ. Policy, 32, 1653–1665, 2004.
Stauffer, D. R. and Seaman, N. L.: Use of four-dimensional data assimilation in a limited-area mesoscale model, Part I: Experiments with synoptic-scale data, Mon. Weather Rev., 118, 1250–1277, 1990.
Stockwell, W. R., Middleton, P., Chang, J. S., and Tang, X.: The second-generation regional acid deposition model chemical mechanism for regional air quality modeling, J. Geophys. Res., 95, 16343–16367, 1990.
Tie, X., Madronich S., Li, G., Ying Z., Zhang R., Garcia, A. R., Lee-Taylor, J., and Liu Y.: Characterizations of chemical oxidants in Mexico City: A regional chemical dynamical model (WRF-Chem) study, Atmos. Environ., 41, 1989–2008, 2007.
U.S. EIA: http://www.eia.gov/cfapps/ipdbproject/iedindex3.cfm?tid=90\&pid=52\&aid=8\&cid=regions\&syid=2005\&eyid=2009\&unit=MMTCD, last access: 23 January 2012.
Vazquez-Alarcon, A., Justin-Cajuste, L., Siebe-Grabach, C., Alcantar-Gonzalez, G., and de la Isla-de Bauer, M. L.: Cadmio, níquel y plomo en agua residual, suelo y cultivos en el Valle del Mezquital, Hidalgo, México, Agrociencia., 35, 267–274, 2001.
Villaseñor, R., Magdaleno, M., Quintanar, A., Gallardo, J. C., López, M. T., Jurado, R., Miranda A., Aguilar, M., Melgarejo, L. A., Palmerín, E., Vallejo, C. J., and Barchet, W. R.: An air quality emission inventory of offshore operations for the exploration and production of petroleum by the Mexican oil industry, Atmos. Environ., 37, 3713–3729, 2003.
Weller, H. G., Tabor, G., Jasak, H., and Fureby, C.: A Tensorial Approach to Computational Continuum Mechanics Using Object-Oriented Techniques, Comput. Phys., 12, 620–631, 1998.

ACPD
12, 15177–15225, 2012

Wild, O., Zhu, X., and Prather, M. J.: Fast-J: Accurate simulation of in- and below cloud photolysis in tropospheric chemical models, J. Atmos. Chem., 37, 245–282, 2000.
Willmott, C. J., Ackleson, S. G., Davis, R. E., Feddema, J. J., Klink, K. M., Legates, D. R., O'Donnell J., and Rowe, C. M.: Statistics for the evaluation of models, J. Geophys. Res., 90, 8995–9005, 1985.
Willmott, C. J. and Matsuura, K.: Advantages of the mean absolute error (MAE) over the root mean square error (RMSE) in assessing model performance, Clim. Res., 30, 79–82, 2005.
Woolley, R. M., Fairweather, M., and Yunardi, Y.: Conditional Moment Closure modelling of soot formation in turbulent non premixed methane and propane flames, Fuel, 88, 393–407, 2009.
World Bank: Global Gas Flaring Reduction, The News Flare, http://go.worldbank.org/D1C50CX1Y0 (last access: January 2012), March–October 2011.
Zambrano García, A., Medina Coyotzin, C., Rojas Amaro, A., López Veneroni, D., Chang Martínez, L., and Sosa Iglesias, G.: Distribution and sources of bioaccumulative air pollutants at Mezquital Valley, Mexico, as reflected by the atmospheric plant Tillandsia recurvata L., Atmos. Chem. Phys., 9, 6479–6494, doi:10.5194/acp-9-6479-2009, 2009.
Zhang, Y. X. and Dubey, M. K.: Comparisons of WRF/Chem simulated O(3) concentrations in Mexico City with ground-based RAMA measurements during the MILAGRO period, Atmos. Environ., 43, 4622–4631, 2009.
Zhang, Y., Dubey, M. K., Olsen, S. C., Zheng, J., and Zhang, R.: Comparisons of WRF/Chem simulations in Mexico City with ground-based RAMA measurements during the 2006-MILAGRO, Atmos. Chem. Phys., 9, 3777–3798, doi:10.5194/acp-9-3777-2009, 2009.

ACPD
12, 15177–15225, 2012

Table 1. Mass flow rates obtained with the E1 approach of the slice method at different heights in the flare simulation domain. The capital S and the number at the right represent the number of the slice. The number in parenthesis shows the height of the slice with respect to the tip of the simulated flame. All the estimates are in kg s^{-1}.

Species	Slice				
	S1 (0 m)	S2 (4 m)	S3 (30 m)	S4 (38 m)	S5 (61 m)
SO_2	4.39	4.50	3.58	3.37	2.73
NO	9.74E-2	9.46E-2	5.25E-2	4.51E-2	3.70E-2
NO_2	3.83E-2	5.46E-2	9.15E-2	8.98E-2	6.88E-2
Soot	1.07E-3	9.26E-4	8.90E-5	8.62E-5	6.11E-5
CO	1.86E-1	1.61E-1	9.20E-2	9.75E-2	1.08E-1
CO_2	15.53	14.50	10.06	9.22	8.57
OH	4.1E-2	2.65E-2	7.78E-4	1.03E-5	9.14E-7

ACPD
12, 15177–15225, 2012

Table 2. Summary of the mass flow rates of combustion air pollutants. Units are in kilograms per second ($kg\,s^{-1}$). F1, F2, and F3 stands for Flare number 1, 2 and 3 respectively. RdF represents the combined reference of Rivera et al. (2009) and de Foy et al. (2009a). * SO_x emissions. E1 and E2 refer to approach 1 and 2 of the slice method respectively.

Species	IMPei*				RdF	This work	
	F1	F2	F3	Total	TIC	E1	E2
SO_2	1.31	6.17E-1	9.57E-3	1.94	4.90 ± 3.80	2.73	1.97
NO_2	–	–	–	–	$2.77E\text{-}1 \pm 8.10E\text{-}2$	6.88E-2	4.69E-2
NO_x	–	–	4.07E-3	–	–	1.05E-01	7.31E-2
VOCs	–	–	2.44E-1	–	–	2.33E-02	2.38E-02
$PM_{2.5}$/Soot	2.35E-4	5.03E-4	2.63E-3	3.37E-3	–	6.11E-05	6.26E-05
CO_2	9.43E-3	1.73E-1	8.27	8.45	–	8.57	7.90
CO	–	–	6.23E-2	–	–	1.08E-01	2.07E-01

ACPD
12, 15177–15225, 2012

Table 3. Performance statistics of the surface variables in the third simulation domain. Location with respect to the center of the city is below the station name.

Station	*T*			WS			WD	
	MAE	RMSE	IOA	MAE	RMSE	IOA	RMSEvec	IOA
CHA (NE)	1.64	1.96	0.94	1.72	2.29	0.86	3.80	0.86
CUA (SW)	1.61	2.00	0.91	1.56	2.00	0.82	2.99	0.75
EAC (NW)	1.90	2.27	0.91	0.97	1.31	0.80	2.29	0.72
MER (C)	2.17	2.63	0.90	0.98	1.34	0.80	2.45	0.75
PLA (SW)	2.00	2.40	0.90	1.05	1.40	0.76	2.22	0.81
TAC (NW)	1.68	2.09	0.92	0.82	1.07	0.85	2.21	0.68
TAH (SE)	2.04	2.34	0.91	1.51	2.01	0.81	3.65	0.54
TLA (NW)	1.93	2.21	0.93	1.02	1.35	0.84	2.68	0.71
TPN (SW)	1.67	2.14	0.90	2.20	2.72	0.53	3.93	0.63
VIF (NE)	1.29	1.66	0.96	1.32	1.75	0.69	2.95	0.70
XAL (NE)	2.51	2.82	0.88	1.39	2.13	0.70	3.24	0.62

ACPD
12, 15177–15225, 2012

Table 4. Model Performance at MILAGRO supersites.

Station	*T*			WS			WD	
	MAE	RMSE	IOA	MAE	RMSE	IOA	RMSEvec	IOA
T0	1.22	1.72	0.94	0.9	1.23	0.82	2.61	0.57
T1	1.79	2.25	0.93	1.87	2.62	0.69	3.38	0.81
T2	1.84	2.29	0.91	1.86	2.44	0.76	3.6	0.88

ACPD
12, 15177–15225, 2012

Table 5. Mass flow rates used in WRF-Chem for the three flares at MHR in Tula. Units are in $kg\,s^{-1}$.

Species	Flare emission rate		
	F1	F2	F3
SO_2	2.01	0.94	0.01
NO_2	5.39E-2	5.39E-2	7.70E-2
NO	2.76E-2	2.76E-2	3.95E-2
NO_x	8.00E-2	8.00E-2	1.10E-1
CO	9.00E-2	9.00E-2	1.10E-1
C_2H_2	1.38E-2	1.38E-2	1.38E-2
C_2H_4	1.99E-4	1.99E-4	1.99E-4
Soot	6.93E-5	6.93E-5	6.93E-5

ACPD
12, 15177–15225, 2012

Table 6. Estimated contribution of flaring activities from TIC, to SO_2 and soot levels at MILAGRO supersites. SO_2 units are ppb and soot units are $\mu g\, m^{-3}$.

Pollutant	Scenario	T0		T1		T2	
		%	Avg	%	Avg	%	Avg
SO_2	High emission	37	2.22	39	2.02	–	–
	Low emission	23	1.42	29	1.48	–	–
Soot	FPRPP+MHR	7	0.29	17	0.25	59	0.25
	Far flame estimate	0.01	4.64E-4	0.03	4.19E-4	0.07	2.73E-4
	overfire	0.14	6.12E-3	0.3	4.50E-3	1.02	3.92E-3

ACPD
12, 15177–15225, 2012

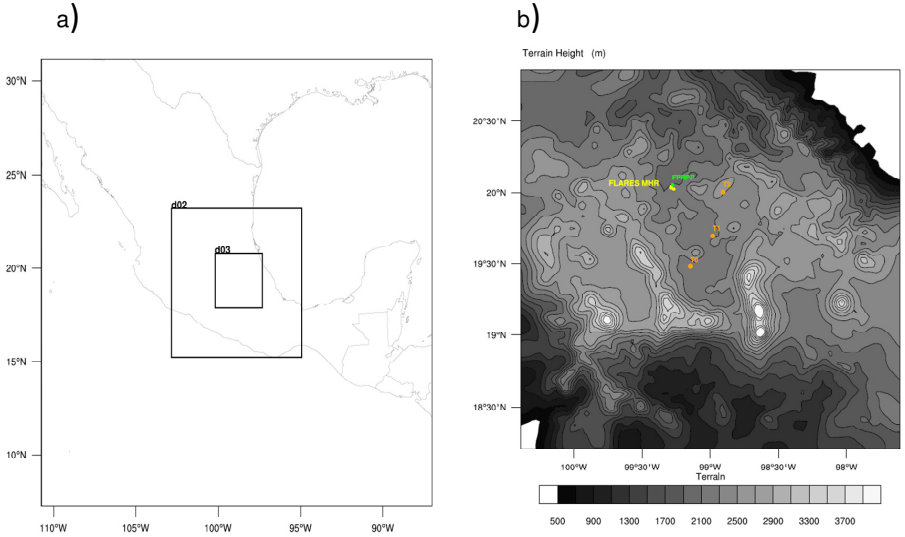

Fig. 1. (a) WRF-Chem model domain. d02 and d03 indicate the number of the nested domain. **(b)** Location of MILAGRO supersites (orange), FPRPP (green) and the elevated flares (yellow) at MHR in d03.

ACPD
12, 15177–15225, 2012

Soot and SO_2 contribution to the supersites in the MILAGRO campaign

V. H. Almanza et al.

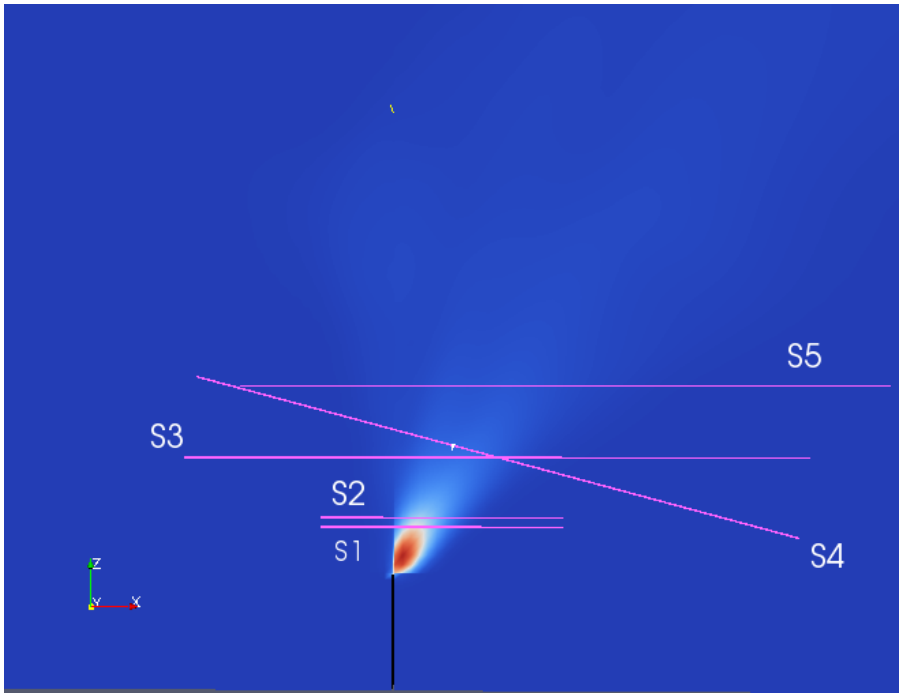

Fig. 2. Average temperature field for the sour gas flare. The location of the cutting slices is in Magenta.

ACPD
12, 15177–15225, 2012

Soot and SO_2 contribution to the supersites in the MILAGRO campaign

V. H. Almanza et al.

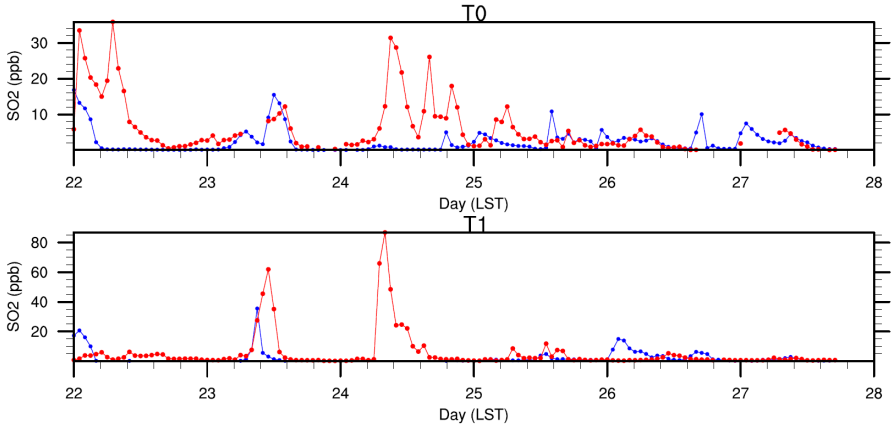

Fig. 3. Comparison of modeled (blue) and observed (red) time series of SO_2 at T0 and T1, for the simulation period.

ACPD
12, 15177–15225, 2012

Soot and SO_2 contribution to the supersites in the MILAGRO campaign

V. H. Almanza et al.

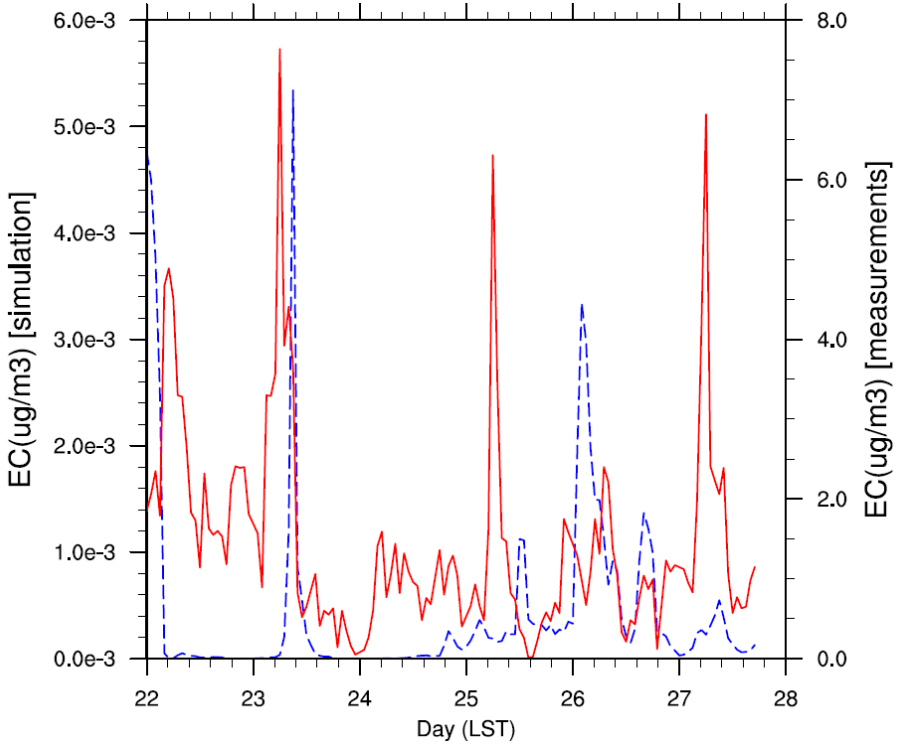

Fig. 4. Time series of EC obtained with the soot mass rate from the combustion model (dashed blue) and measurements (red) at T1 site.

ACPD
12, 15177–15225, 2012

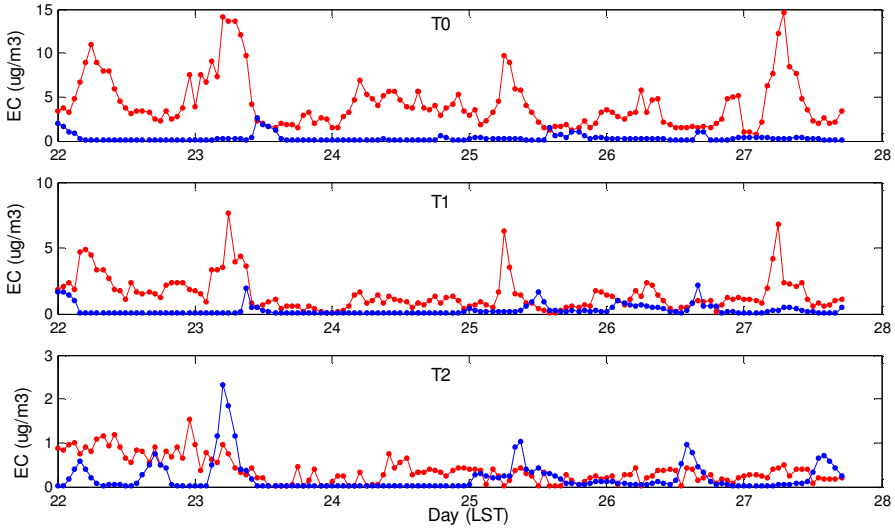

Fig. 5. Model concentration (blue) and measurements (red) of EC for the simulation period. T0 (upper panel); T1 (middle panel) and T2 (bottom panel).

ACPD
12, 15177–15225, 2012

Soot and SO_2 contribution to the supersites in the MILAGRO campaign

V. H. Almanza et al.

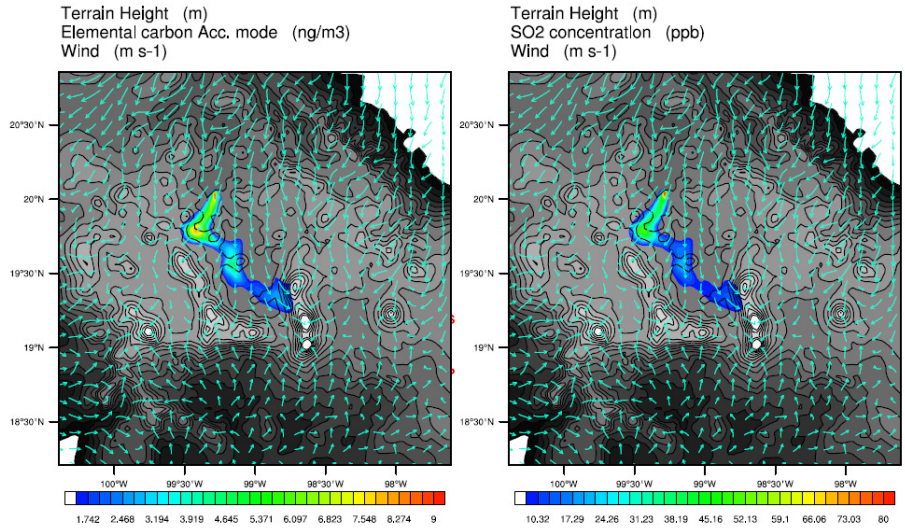

Fig. 6. Simulated plume and wind fields at the surface for 23 March at 12:00 LST. Left Pannel Soot; Right Pannel SO_2.

ACPD
12, 15177–15225, 2012

Soot and SO_2 contribution to the supersites in the MILAGRO campaign

V. H. Almanza et al.

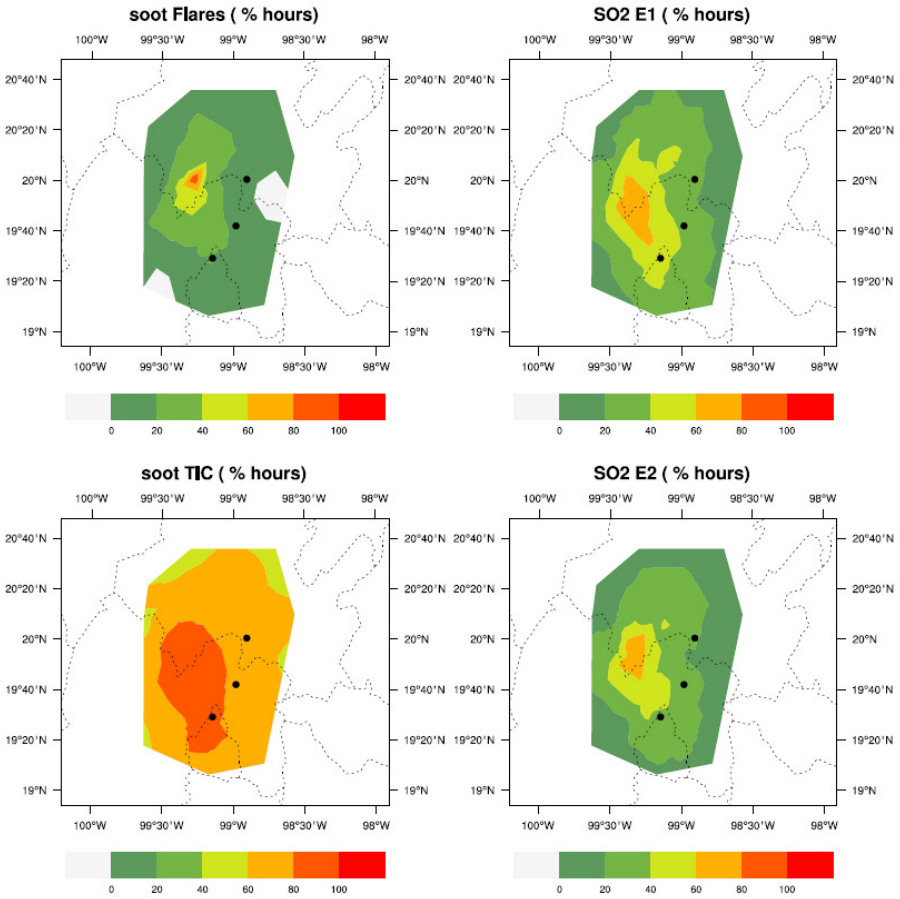

Fig. 7. Suggested contribution of primary pollutants in the period from 22 March to 27 March of 2006. Black dots show the location of the three supersites.

ACPD
12, 15177–15225, 2012

Soot and SO_2 contribution to the supersites in the MILAGRO campaign

V. H. Almanza et al.